ACS SENSORS

pubs.acs.org/acssensors
Article

Surface-Enhanced Raman Scattering Monitoring of Tryptophan Dynamics in 3D Pancreatic Tumor Models

Pablo S. Valera,[○] Margarida Henriques-Pereira,[○] Marita Wagner, Vítor M. Gaspar, João F. Mano, and Luis M. Liz-Marzán*

Cite This: *ACS Sens.* 2024, 9, 4236−4247

ABSTRACT: In the intricate landscape of the tumor microenvironment, both cancer and stromal cells undergo rapid metabolic adaptations to support their growth. Given the relevant role of the metabolic secretome in fueling tumor progression, its unique metabolic characteristics have gained prominence as potential biomarkers and therapeutic targets. As a result, rapid and accurate tools have been developed to track metabolic changes in the tumor microenvironment with high sensitivity and resolution. Surface-enhanced Raman scattering (SERS) is a highly sensitive analytical technique and has been proven efficient toward the detection of metabolites in biological media. However, profiling secreted metabolites in complex cellular environments such as those in tumor−stroma 3D *in vitro* models remains challenging. To address this limitation, we employed a SERS-based strategy to investigate the metabolic secretome of pancreatic tumor models within 3D cultures. We aimed to monitor the immunosuppressive potential of stratified pancreatic cancer−stroma spheroids as compared to 3D cultures of either pancreatic cancer cells or cancer-associated fibroblasts, focusing on the metabolic conversion of tryptophan into kynurenine by the IDO-1 enzyme. We additionally sought to elucidate the dynamics of tryptophan consumption in correlation with the size, temporal evolution, and composition of the spheroids, as well as assessing the effects of different drugs targeting the IDO-1 machinery. As a result, we confirm that SERS can be a valuable tool toward the optimization of cancer spheroids, in connection with their tryptophan metabolizing capacity, potentially allowing high-throughput spheroid analysis.

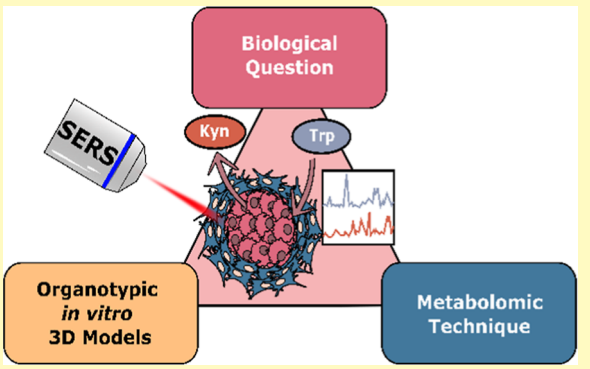

KEYWORDS: *SERS, plasmonics, tumor spheroids, pancreatic cancer, tryptophan*

INTRODUCTION

The rewiring of tumor metabolism has been recognized as one of the emerging hallmarks of cancer.[1] During tumor progression, metabolism-based communication represents a biochemical mechanism by which tumors reprogram the host machinery. In this intricate niche, cancer cells and stromal elements orchestrate bidirectional interactions that have a profound impact on the properties of the tumor microenvironment (TME).[2,3] This adaptive process not only enables tumors to endure unsuitable conditions, but also supports growth and survival while concurrently impairing antitumor immunity.[4] As a result, the unique metabolic characteristics of tumors have motivated significant and exciting research in cancer therapeutics.[5] Recent evidence[6−8] suggests that targeting metabolic pathways in pancreatic ductal adenocarcinoma (PDAC) may offer attractive therapeutic opportunities. Pancreatic cancer cells exhibit extensive metabolic plasticity, driven by the unique physiology of its TME. The human PDAC niche is characterized by a desmoplastic stroma with extensive fibrosis and extracellular matrix deposition, articulated by cancer-associated fibroblasts (CAFs), and generating highly hypoxic and immunosuppressive conditions within the tumor.[9,10] One of the primary pathways through which PDAC modulates immune suppression is via tryptophan (Trp) catabolism.[11] This mechanism is mediated by enzymes such as indoleamine 2,3-dioxygenase (IDO-1) and tryptophan 2,3 dioxygenase (TDO), which convert Trp into kynurenine (Kyn) metabolites. The IDO-1 enzyme, typically expressed in a tissue-specific manner under normal circumstances, can be significantly upregulated in response to cytokines released during inflammation. The produced kynurenine metabolites, in turn, regulate immune cell function by activating the aryl hydrocarbon receptor (AhR).[12] This kynurenine/AhR pathway is involved in the generation of regulatory T-cells (T_{regs}) and in the development of an immunomodulatory phenotype in

Received: May 20, 2024
Revised: July 10, 2024
Accepted: July 12, 2024
Published: July 19, 2024

dendritic cells, which facilitate immunosurveillance escape and promote tumor development.[13] The relevance of IDO-1 in the induction of immune tolerance in PDAC has raised interest in IDO-1 inhibitors, such as epacadostat, and their combinations with other immunotherapies (e.g., immune checkpoint inhibitors). Despite its therapeutic potential in PDAC, its safety and tolerability remain to be investigated.[14] For this reason, rapid and accurate monitoring of the metabolic dynamics within the TME is essential to analyze the response of tumors to therapeutic intervention or to identify novel therapeutic strategies. However, there is a lack of suitable alternatives for fast monitoring of metabolites without using invasive and cumbersome procedures that often require sample loss.

Traditional techniques in biomedical research, such as liquid chromatography−coupled mass spectrometry (LC−MS) and nuclear magnetic resonance (NMR), are typically time-consuming and expensive, involve destructive procedures for LC−MS and have limited sensitivity in the case of NMR.[15,16] In response to these challenges, surface-enhanced Raman spectroscopy (SERS) offers the possibility to evaluate tumor metabolomics in a fast, cost-effective, sensitive, and label-free manner. SERS reveals the vibrational fingerprints of molecules adsorbed onto plasmonic nanostructures, by enhancing their specific Raman scattering signals. Recent studies have demonstrated that SERS is a useful technique for monitoring cancer metabolic communications.[17−19] However, profiling of secreted metabolites in physiologically relevant platforms requires further improvement if SERS is to be widely applied in cancer research. Traditional two-dimensional (2D) cell cultures, while informative, offer an overly simplified view of biological processes, failing to fully capture the complex interactions and spatial arrangements present in native tissues.[20] Therefore, in an effort to accurately reproduce key features of human solid tumors, three-dimensional (3D) *in vitro* cell culture models have been widely explored.[21,22] 3D *in vitro* models provide a unique platform to investigate cancer dynamics and metabolism in a preclinical setting because they recapitulate cell−cell interactions, gene expression and nutrient/oxygen gradients found in solid tumors.[23]

We present herein a SERS-based strategy to investigate the metabolic Trp signature of 3D stratified microenvironment spheroid models (STAM), which recapitulate the unique PDAC microenvironment. Such a model was previously devised to exhibit a stratified architecture with a core of pancreatic cancer cells (PANC-1) and a surrounding stromal compartment populated by CAFs.[24] Recognizing IDO-1 as a promoter of immune evasion in PDAC, we focused on the immunosuppressive potential of STAM spheroids by monitoring the metabolic conversion of Trp into Kyn by the IDO-1 enzyme. In addition, we aimed to unravel the dynamics of Trp consumption and to correlate them with the size, temporal evolution, and composition of the spheroids, finally assessing the effects of different drugs targeting the IDO-1 machinery.

Overall, our results advocate for the continued exploration and integration of SERS into biomedical research, positioning it as a powerful and versatile tool for probing cellular processes and unraveling drug responses within the context of biomimetic 3D cellular models. The promising attributes of SERS may help advancing our understanding of cancer biology and therapeutic interventions.

EXPERIMENTAL SECTION

Materials. Aluminum foil (ALUGRAM RP-18W) and tetrachloroauric (III) acid trihydrate ($HAuCl_4 \cdot 3H_2O$) (≥99.9%, trace metal basis) were purchased from Alfa Aesar. Standard Photopolymer resin by Elegoo, SYLGARD 184 Silicone Elastomer Kit of Dow, and enamel acrylic spray was purchased from Pintyplus Evolution. Trisodium citrate and silver nitrate ($AgNO_3$), as well as commercial samples of tryptophan (Trp), kynurenine (Kyn), hemin, epacadostat, and interferon (IFN)-ϒ, were supplied by Sigma-Aldrich.

Cell Culture. Ultralow adhesion (ULA) U-bottom 96-well plates (Corning, 7007), 6/12/24-well plates (Thermo Scientific), Corning Transwell Inserts (Sigma-Aldrich), fetal bovine serum (FBS, E.U. approved, South America origin), Dulbecco's modified Eagle medium-high glucose (DMEM-HG), phosphate buffered saline without Ca^{2+} and Mg^{2+} (D-PBS, pH = 7.4), antibiotic-antimycotic (ATB, Gibco—10,000 U mL^{-1} of penicillin, 10,000 μg mL^{-1} of streptomycin, and 25 μg mL^{-1} of amphotericin B), trypsin-ethylenediaminetetraacetic acid (EDTA) detaching solution, gelatin form porcine skin type A, and hyaluronic acid (MW ≈ 1.5×10^6 to 1.8×10^6 Da) were obtained from Merck-Sigma. MSC-GRO Low-Serum Complete Mesenchymal Stem Cell Medium, was obtained from Neuromics (Neuromics, Inc., MN, USA). Lactate dehydrogenase (LDH) cytotoxicity assay kit was from Thermo Scientific. TaqMan gene expression assay of glyceraldehyde-3-phosphate dehydrogenase (GAPDH) and indoleamine 2,3-dioxygenase (IDO-1) were supplied by Thermo Fisher Scientific. Proteome profiler human cytokine array kit was purchased from Bio-Techne R&D Systems. L-Tryptophan and L-kynurenine enzyme-linked immunoassay (ELISA) kits were purchased at ImmuSmol. All solutions, except $HAuCl_4$, were prepared immediately before use. Purified Milli-Q water was used in all experiments (Millipore, 18.2 MΩ cm).

Synthesis of Citrate Au Nanoparticles (30 nm). Gold nanoparticles (AuNPs) stabilized with citrate were synthesized using a previously described seeded growth method.[25] In brief, 150 mL of a 2.2 mM trisodium citrate aqueous solution was heated to boiling with vigorous stirring. After 15 min, 1 mL of a 25 mM $HAuCl_4$ solution was added to the boiling mixture and allowed to react for 10 min. The reaction mixture was then cooled to 90 °C, and 1 mL of a 25 mM $HAuCl_4$ aqueous solution was added. After additional 30 min, the $HAuCl_4$ addition step was repeated. Subsequently, the sample was diluted by removing 55 mL of the mixture and adding 53 mL of water along with 2 mL of a 60 mM sodium citrate solution. This resulting solution acted as a seed, and the process (addition of 2 mL of 25 mM $HAuCl_4$ every 30 min followed by dilution) was repeated six times to obtain 30 nm gold nanoparticles. To remove excess reactants, colloidal dispersions underwent centrifugation at 1520*g* for 20 min, followed by redispersion in an equal volume of water.

Drying Drop Substrates. To produce substrates with a random distribution of AuNPs, 2 μL of a 2 mM AuNP solution was drop-casted onto an aluminum foil substrate. After drying at room temperature in air (approximately 1 h), 2 μL of selected cell-derived supernatants was casted onto the freshly prepared SERS substrates and allowed to dry completely before conducting SERS measurements.

Fabrication of PDMS-Based 96 Well-Plate Lids. 3D patterns were fabricated on light-curable resin, with the desired geometry at micron-scale resolution, by means of 3D stereolithography (SLA) printing. This method integrates traditional PDMS soft lithography with SLA 3D printed molds, following a common approach for micropatterned silicon masters. Initially, 3D designs for the well-plate lids were created using the Tinkercad online tool. These models were then 3D printed using the Anycubic Photon Mono printer and Standard Photopolymer resin. After printing, the resin-based masters were cleaned with 2-propanol and cured under a 365 nm UV lamp. Subsequently, the resin was coated with a thin layer of enamel to improve the PDMS curing process, as previously described.[26] Polydimethylsiloxane was prepared at a 10:1 weight ratio of base to curing agent. The resulting solution was poured into the resin master

https://doi.org/10.1021/acssensors.4c01210
ACS Sens. 2024, 9, 4236−4247

and degassed to remove air bubbles. Following curing at 70 °C, the replica-molded layer was trimmed and cleaned with 70% ethanol.

SERS Measurements. Supernatants from various biological assays were collected and 2 μL of the liquid was poured onto a plasmonic substrate. Following solvent evaporation, SERS spectra were measured using substrates fabricated by drop casting. All experimental conditions were replicated in a minimum of three independent cell assays, each applied to three separate plasmonic substrates. Subsequently, SERS spectra were acquired using an InVia Reflex Raman microscope from Renishaw plc. This instrument comprises an optical microscope (Leica) with an *XYZ* scanning stage connected to a high-throughput Raman spectrometer equipped with a 1024 × 512 front-illuminated CCD detector and a grating of 1200 grooves mm^{-1} for 785 nm excitation. A line-shaped 785 nm laser source (maximum 190 mW) was used, operating in static mode with standard confocality through a long-distance 50× objective (numerical aperture NA = 0.5), with an integration time of 1 s at 15.15 mW (10% of the maximum power).

The *XYZ* scanning stage allowed for *Z*-axis control to focus the laser on the plasmonic substrate's surface, while *XY* displacement determined the laser beam position over the substrate. Once focus was achieved on a specific area chosen from an optical image, SERS measurements were conducted as described above. Additionally, *XY* scanning enabled the acquisition of multiple SERS spectra at different positions. As a standard procedure, 25 points from various substrate areas were measured each time, to sample different spots on the plasmonic substrate. This method was also used to generate a SERS map of the scanned area, aiding in the identification of substrate regions exposed to the analyte solution and recording the characteristic SERS fingerprint of adsorbed molecules. All represented SERS spectra are normalized to the highest intensity peak, to overcome intersubstrate absolute intensity variations. The SERS spectra shown throughout the study are the average from 25 individual spectra, except for PDMS measurements, in which the average spectra derive from 100 measurements.

Cell Culture. All cell lines used in this study, including PANC-1 and pancreatic CAFs, were obtained from ATCC. PANC-1 cells were cultured in DMEM-HG medium supplemented with 10% FBS and 1% (v/v) penicillin−streptomycin, whereas pancreatic CAFs were cultured in MSC-GRO Low serum media supplemented with 10% fetal calf serum and 1% (v/v) penicillin−streptomycin. For cell passaging, adherent cells on a T-75 flask were detached using 1% trypsin−EDTA solution and incubated for 3 min after rinsing with PBS solution. After detachment, cells were diluted 1:3 and resuspended in cell media before being seeded into a fresh T-75 flask. Cell counting was performed by mixing 10 μL of cell suspension with 10 μL of Trypan Blue and loading the mixture into a Neubauer chamber.

Generation of 3D Cancer Models. To fabricate 3D PDAC models incorporating living cells, we utilized superhydrophobic surfaces and visible LED light-mediated photo-cross-linking, following a previously reported method.[24]

Additionally, we generated monotypic spheroids (consisting solely of cancer cells or fibroblasts) and stratified microenvironment spheroids (STAM, containing both cancer cells and CAFs in a core−shell arrangement) using the liquid overlay technique (LOT). For monotypic PANC-1 and CAF spheroids, cellular suspensions with varying spheroid sizes (small: 10,000 cells; medium: 20,000 cells; large: 50,000 cells) were prepared and seeded into 96-well ultralow attachment (ULA) plates to form 3D spheroids via LOT.

To generate heterotypic 3D STAM, we employed a two-step strategy as previously described.[24] In the initial phase, a 3D spheroid core consisting of PANC-1 cells was cultured *in vitro* as described above. On day 7 of maturation, a suspension of human pancreatic stellate CAFs was added to the wells containing the tumor core spheroid, to establish the stratified 3D heterotypic model [without extracellular matrix (ECM) components]. In all tumor−stroma models, CAFs represented 80% of the tumor mass, to better mimic the stromal occupancy ratio observed *in vivo*.

All generated 3D PDAC models were cultured under a 5% CO_2 atmosphere at 37 °C. Morphometric parameters, including size and circularity, of the 3D *in vitro* PDAC models were evaluated at days 3, 7, and 14 of culture, using optical contrast microscopy with an inverted microscope (Zeiss Primovert, Carl Zeiss, Germany). Image circularity and perimeter analysis were performed using the open-source software ImageJ (Fiji package, NIH, USA) with a macro extension developed by Ivanov and colleagues.[27] To acquire SERS measurements of spheroid-derived supernatants, 100 μL of spheroid-conditioned media was collected at the desired time points. The spheroids were maintained in culture with the addition of fresh media. Supernatants were collected at selected time points (10, 14, and 21 days, and after drug treatment). For each SERS measurement, 2 μL of the supernatant was used. The supernatant samples were stored at −20 °C and protected from multiple freeze−thaw cycles.

IDO-1 Activity Stimulation and Inhibition. Spheroids of PANC-1, CAFs, and STAM were subjected to treatment with either hemin (IDO-1 cofactor) or epacadostat (IDO-1 inhibitor) on day 14 postseeding in 96-well round-bottom ultralow attachment (ULA) plates. The exposure to hemin varied in time and concentration: 10 μM of hemin for 24 and 48 h; 20 μM of hemin for 24 h. Regarding epacadostat, all concentrations (10, 75, and 100 μM) were tested over a 48 h period. In experiments where Trp was additionally introduced to the spheroids, it was administered simultaneously with the drug treatment.

Q-RT-PCR. In IDO-1 gene expression assays, the spheroids were homogenized by pipetting up and down, and RNA extraction was performed using the PureLink RNA Mini Kit from Invitrogen. To generate cDNA from 1 μg of total RNA, the qScript cDNA Supermix from Quanta was employed (ref 95048). Quantitative real-time PCR (Q-RT-PCR) was conducted by combining 2 μL of the cDNA sample (0.01 μg/μL) with 18 μL of a mixture containing Maxima RT buffer and the TaqMan Gene Expression Assay, in a 96-well plate. Thermo Fisher Scientific TaqMan probe for IDO-1 (Hs00984148_m1) was used. Glyceraldehyde-3-phosphate dehydrogenase (human: Hs02786624_g1) served as the standard for normalizing the Q-RT-PCR results.

LDH Cytotoxicity Assay. Cell viability was assessed through LDH cytotoxicity assay. LDH, an enzyme present in all cell types, is released into the cell culture medium when the plasma membrane is damaged. The assays were performed following the manufacturer's protocol, which involved adding 50 μL of cell media from the experimental conditions to a 96-well plate. The absorbance of these solutions was then measured at 490 and 680 nm using a Thermo Scientific Varioskan Flash plate reader. Cell viability percentage was calculated as follows

$$\text{citotoxicity}(\%): \frac{A_{490}[\text{experiment}] - A_{490}[\text{low control}]}{A_{490}[\text{high control}] - A_{490}[\text{low control}]}$$

Live & Dead Staining. Viability assessment was conducted using a live/dead cell assay. In brief, 3D tumor spheroids were subjected to incubation with calcein AM (1:200) and propidium iodide (1:100) in PBS, under standard culture conditions (5% CO_2 at 37 °C) for a duration of 30 min. Following a thorough wash with PBS, 3D tumor models were observed using a widefield fluorescence microscope (Fluorescence Microscope Zeiss, Axio Imager 2, Carl Zeiss, Germany).

Cytokine Array Assay. Proteome Profiler Human Cytokine Array assays (R&D Systems, ARY005B) were conducted in accordance with the manufacturer's instructions. Briefly, supernatants obtained from spheroid or 2D cell cultures were collected and applied to the array membranes, then incubated overnight at 4 °C. After washing the membranes, they were incubated with a streptavidin-HRP-coupled antibody (diluted at 1:2000) for 30 min at room temperature, followed by development using Chemi-Reagent Mix. Images were captured and visualized using the LI-COR Odyssey Fc imaging system, and dot integrated densities were quantified using ImageJ software. Integrated density was calculated as the product of the area of a manually selected region of interest and its mean pixel intensity.

https://doi.org/10.1021/acssensors.4c01210
ACS Sens. 2024, 9, 4236−4247

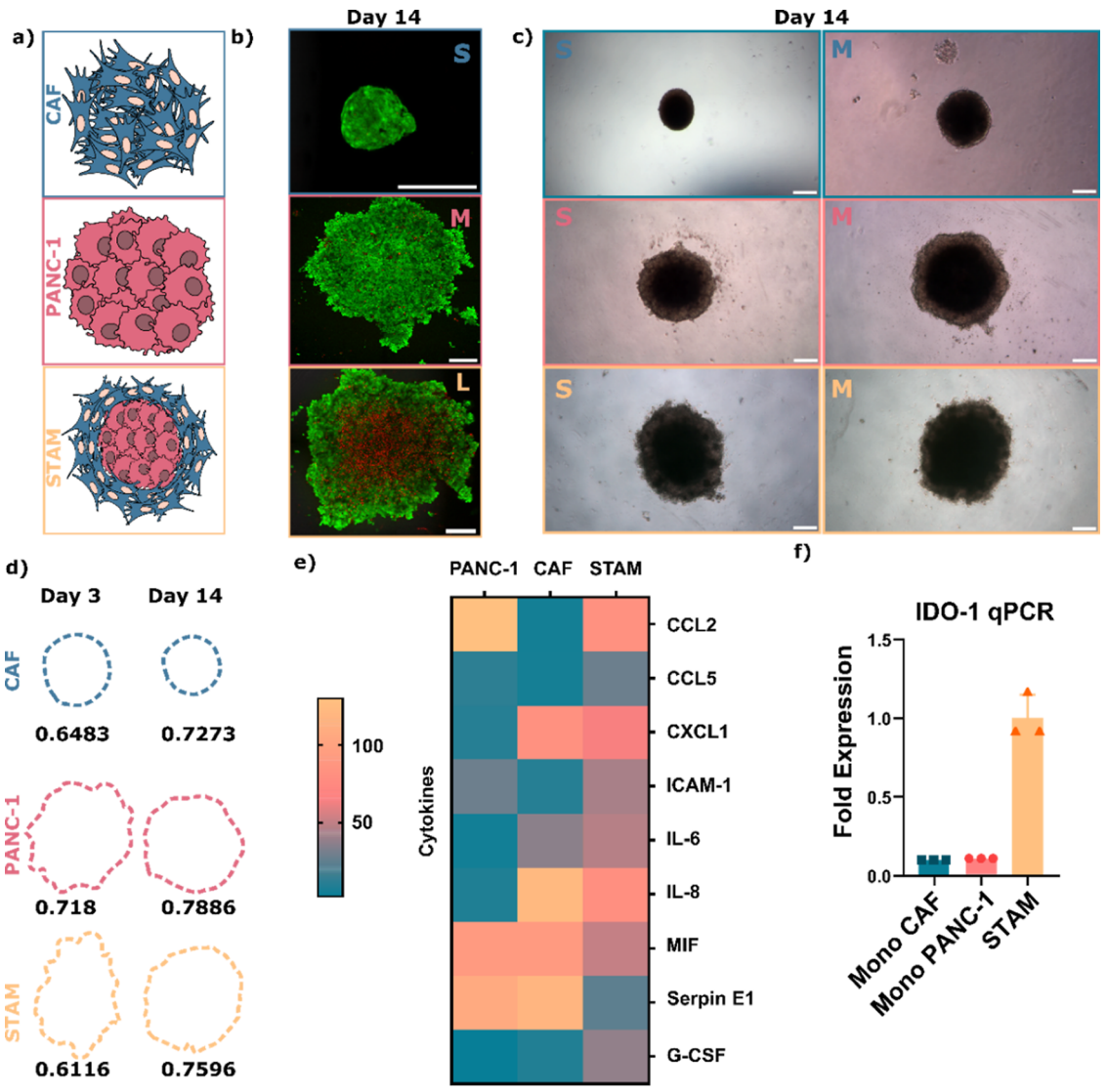

Figure 1. (a) Scheme depicting the strategy followed to create spheroids from monocultures of CAFs and PANC-1, and the stratified coculture of both populations (STAM). (b) Live & dead staining pictures of S, M, and L-sized CAFs, PANC-1 and STAM spheroids. Scale bars: 300 μm. (c) Optical contrast micrographs of CAFs, PANC-1, and STAM spheroids, at S and M sizes, on day 14 after seeding. Scale bars: 300 μm. (d) Circularity calculations of M-sized spheroids at day 3 and day 14 after seeding, obtained as the average of 3 spheroids circularity calculations for each spheroid type and time point. (e) Cytokine array-derived heatmap analysis of monoculture spheroids of PANC-1, CAF and STAM spheroids. Significantly increased secretion of CXCL1, IL-6, and IL-8 was observed in fibroblast spheroids. (f) IDO-1 RT-Q-PCR analysis comparing expression levels in monoculture and STAM spheroids. Data is presented as mean ± SD, n = 3, technical replicates and normalized to GAPDH gene.

ROIs were defined by manually outlining a region around each dot on the membrane. Additionally, the integrated density values of the dots from each sample were normalized to the integrated density of the control dots on each respective membrane.

ELISA Assay. Quantification of metabolites secreted by various 3D PDAC models, including Trp and kynurenine was accomplished by ELISA (ImmuSmol). Briefly, at designated time points (7, 10, 14 days and after drug treatment), the culture medium (n = 3, technical replicates) from each condition was collected and stored at −80 °C. Quantification of human PDAC biomolecular markers was carried out using sandwich ELISA, following the instructions of the manufacturer. Absorbance readings were obtained using a multimodal Synergy HTX microplate reader (BioTek Instruments, USA).

Scanning Electron Microscopy. Scanning electron microscopy (SEM) images were acquired on a JSM-IT800HL (JEOL, Japan) at 3−5 kV under high vacuum. To minimize charging, the top containing the dried colloid droplet of the PDMS lid support was cut off, leaving the sensing interface unchanged. The colloid droplet on the PDMS lid support was connected to the holder via copper tape, further reducing charging. The images were recorded by simultaneously using a secondary electron detector and a top-view backscatter electron detector (BSE detector, scintillator-photomultiplier detector design). By collecting images from these two detectors and without metal coverage we could classify the areas of nanoparticles and PDMS.

Transmission Electron Microscopy. Transmission electron microscopy (TEM) images were taken on a JEOL JEM-1400PLUS 241 transmission electron microscope operating at 120 kV. The nanoparticles were washed by centrifugation and additional 3 times using Milli-Q water (5 min, 6000 rpm), resuspended in Milli-Q water and drop-casted onto a TEM grid (carbon film 400 mesh copper, CF400-CU Electron Microscopy Sciences), and dried overnight.

UV−Vis−NIR Spectroscopy. Extinction spectra of colloidal dispersions were recorded using an Agilent 8453 UV/vis spectrophotometer, with polystyrene cuvettes. For the extinction spectra of

https://doi.org/10.1021/acssensors.4c01210
ACS Sens. 2024, 9, 4236−4247

plasmonic substrates, a Cary 500 UV−vis spectrophotometer (Agilent) was employed.

Statistical Analysis. Bar graphs and point graphs display mean value ± SD. Unpaired Student's *t* tests were conducted for single mean comparisons. Significance levels were assigned as follows: $*P < 0.05$, $**P < 0.01$, $***P < 0.001$. Statistical analyses and graphs were performed using the GraphPad Prism 8.3.0 software.

RESULTS AND DISCUSSION

Inducing the Expression of IDO-1 Enzyme in 3D Cultures of Stratified Spheroids. We first established biomimetic 3D *in vitro* tumor−stroma models for metabolic monitoring. Stromal elements act as key orchestrators within the tumor ecosystem, responding to activating signals from their interactions with cancer cells. The conversion of tryptophan into kynurenine within the TME can potentially establish an immune suppressive niche, thereby facilitating the evasion of immune surveillance by the tumor. We built upon previous studies showcasing spheroids as suitable 3D culture platforms for a first approximation to study TME metabolic communications in 3D. For this, different 3D spheroid models, encompassing monocultures of either CAFs or cancer cells (PANC-1), as well as a coculture of both populations, were bioengineered. Cells were cultured in monoculture or coculture within low-attachment cell culture plates, fostering the formation of 3D spheroids through cell-to-cell aggregation. For the coculture 3D system, we employed stratified pancreatic cancer−stroma spheroids (STAM), characterized by a central core of cancer cells surrounded by a stromal shell (all three spheroid models are illustrated in Figure 1a). For further optimization of the spheroids, we studied the effects of cellular density and days in culture on spheroid formation and associated cytotoxicity. Therefore, we generated three spheroid sizes and performed live and dead (LD) staining assays: small (S), medium (M), and large (L), as described in the Experimental Section (see also Figure 1b). In the case of STAM spheroids, we maintained a 1:4 ratio between cancer cells and fibroblasts, mimicking the naturally occurring desmoplastic TME where CAFs can significantly outnumber cancer cells.[28] The LD staining of the spheroids at day 14 revealed no cytotoxicity in S and M sizes,[24] whereas a big necrotic core was observed in L-sized STAM spheroids, prompting us to focus on S and M models, as more appropriate models for Trp catabolic studies. Size distributions for S and M spheroids are displayed in Figure S1. Optical microscopy images captured at various time points (day 3, 7, and 14) and sizes (S and M) facilitated a visual evaluation of spheroid growth (Figures S2 and 1c). As illustrated in Figure 1c, at day 14 after seeding both S and M models for the monoculture of PANC-1 and CAFs, as well as the stratified coculture of both cell types, showed a higher morphological homogeneity. For quantification, we present in Figure 1d a comparative analysis of circularity calculations for M-sized spheroids between days 3 and 14 after seeding. Visual inspection of the optical images revealed a significant increase in circularity at day 14, with the CAF monoculture exhibiting a notably more rounded shape. This comprehensive study captured the dynamic changes within the spheroid models over the course of the experiment, providing valuable insights into their growth and morphological characteristics.

After generating various spheroids and studying their optimal sizes and times in culture, we aimed to effectively induce the expression of the IDO-1 enzyme in cancer cells, thereby triggering the targeted metabolic conversion between Trp and Kyn. In previous studies,[17] external stimuli such as IFN-γ were used to induce the expression of the enzyme. We devised instead a model wherein CAFs, which are known to contribute to inflammation in the TME, were responsible for producing proinflammatory signals. These signals were expected to prompt the expression of IDO-1 in cancer cells within the 3D STAM models, potentially serving as an immune suppressive mechanism. To support this hypothesis, we conducted an analysis of cytokines produced by CAFs, using a membrane sandwich immunoassay-based cytokine array, evaluating PANC-1, CAF and STAM spheroids. As shown in Figure 1e, the secretomes derived from fibroblasts and from the coculture were significantly enriched in CXCL1, IL-6, and IL-8. In the orchestration of the inflammatory response, CXCL1, IL-6, and IL-8 emerge as pivotal pro-inflammatory players, attracting and activating immune cells as neutrophils to the infection or injury site, and enhancing their pathogen-clearing capabilities.[29−31] In addition, evaluation of IDO-1 showed negligible expression across the monoculture 3D models. However, when both cell populations were cultured together, IDO-1 expression was observed (Figure 1f). This observation confirmed our hypothesis that IDO-1 expression is induced within the coculture system, likely in response to interactions between cancer cells and CAFs, potentially mediated by the proinflammatory secreted profile of the latter.

Monitoring the Conversion between Tryptophan and Kynurenine in 2D and 3D Pancreatic Models. After generating suitable 3D monoculture and coculture tumor−stroma models in which we can induce the expression of the IDO-1 enzyme on-demand, we evaluated the use of SERS as a metabolomic technique, to monitor the tryptophan catabolism pathway. We studied the Raman signals of solid Kyn and Trp samples (Figure S3a).[17,32] When selecting the plasmonic substrate, we focused on facilitating high-throughput measurements and thus opted for drop-casting of colloidal nanoparticles (NPs) on aluminum film supports. This procedure offers simplicity, while achieving a competitive Raman signal enhancement and maintaining sufficient substrate homogeneity (Figure S3b,c). Drop-casted citrate-coated Au nanospheres (diameter ≈ 30 nm) enabled us to detect both tryptophan and kynurenine at 100 μM in HBSS (Figure S3d). Morphological and optical characterization of AuNPs is also provided in Figure S3. These substrates were first applied to monitoring tryptophan catabolism in 2D environments. We aimed to determine the limit of detection (LOD) for the target metabolites in a simplified salt solution—HBSS and subsequently in DMEM-HG (pure spectra for both solutions are shown in Figure S4). SERS spectra for three different concentrations (100, 20, and 10 μM) of tryptophan and kynurenine in HBSS and DMEM-HG are presented in Figure S5. Spectra in HBSS revealed the characteristic peaks of both metabolites at all three concentrations, whereas a more modest performance was obtained for kynurenine in the complex cellular medium, with a low signal at 20 μM and no signal at 10 μM. This discrepancy suggests a higher LOD for kynurenine compared to tryptophan, which can be attributed to different affinities for the plasmonic nanoparticles and interferences between media components and the metabolite. It is important to consider the difficulty of establishing absolute correlations between metabolite concentrations and SERS peak absolute intensities, thereby emphasizing the challenges of applying SERS as a semiquantitative technique.

https://doi.org/10.1021/acssensors.4c01210
ACS Sens. 2024, 9, 4236−4247

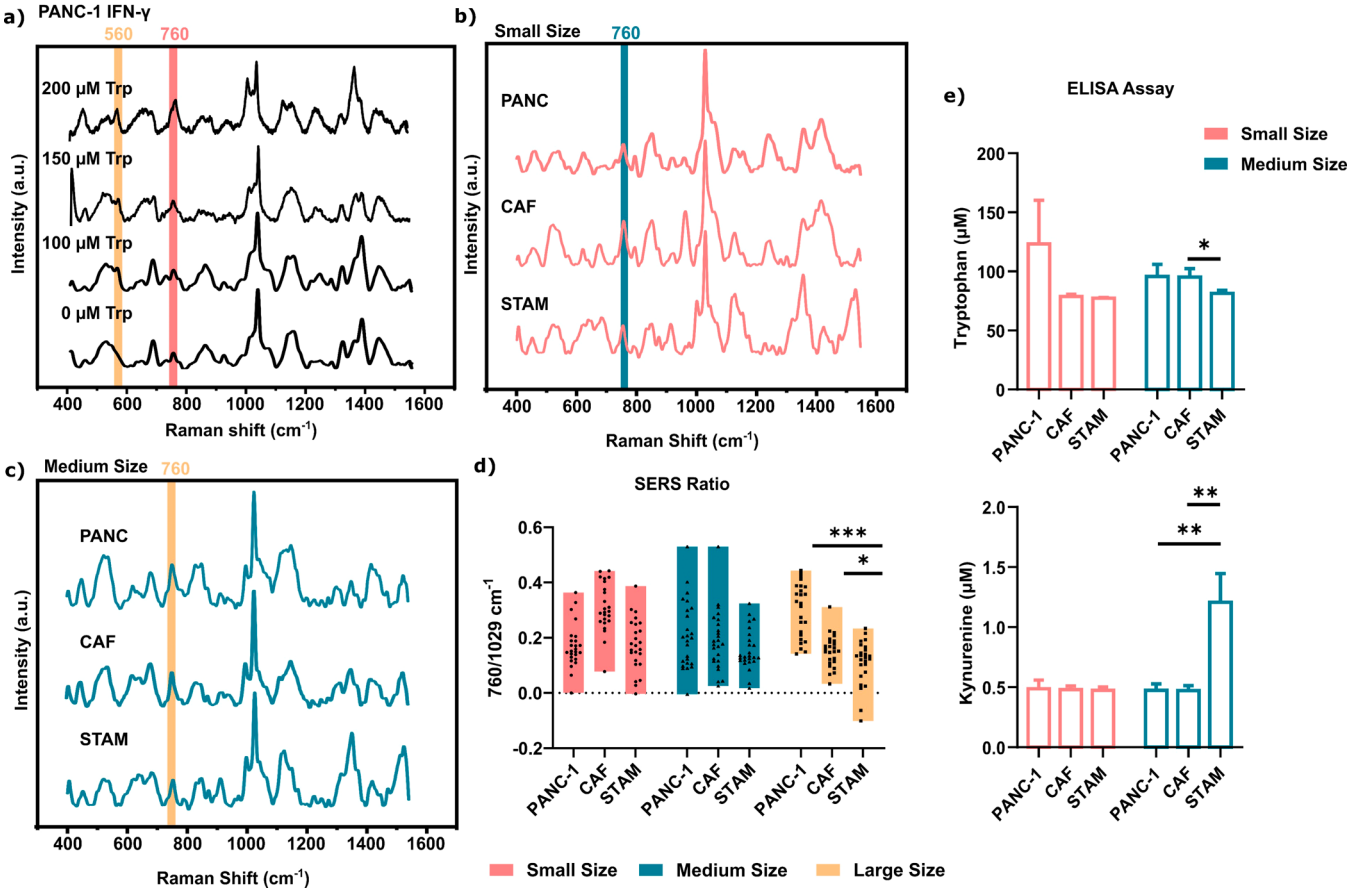

Figure 2. (a) SERS spectra of PANC-1 cells cultured in the presence of IFN-γ, with increasing tryptophan concentrations: 0, 100, 150, and 200 μM for 48 h. The tryptophan peak at 760 cm^{-1} persists, whereas a signal related to kynurenine emerges at 560 cm^{-1}. (b) SERS spectra from monocultures and STAM spheroids of S size, on day 14. (c) SERS spectra illustrating monoculture and STAM M size spheroids on day 14. (d) Ratio between the peaks at 760 and 1029 cm^{-1} based on 25 SERS spectra from S, M and L spheroids. (e) Results of tryptophan and kynurenine ELISA assays for spheroids of different sizes on day 14. Data presented as mean ± SD *P < 0.05, **P < 0.01, ***P < 0.001.

Subsequently, we attempted to measure the Trp-to-Kyn conversion in our PANC-1 model. Control PANC-1 cells were cultured with increasing concentrations of tryptophan (0, 100, 150, and 200 μM) for 48 h. The resulting SERS spectra in Figure S6a revealed heightened intensities of the 760 cm^{-1} peak with increasing tryptophan concentrations, whereas kynurenine-associated signals remained inconclusive. However, when cells were treated with IFN-γ to induce the expression of the IDO-1 enzyme for 48 h, this pattern was altered, with a reduction of the main Trp peak and emergence of the Kyn signal at 560 cm^{-1}, particularly at 200 μM tryptophan (Figure 2a). The Trp/Kyn ratio was calculated from the corresponding ratio between the SERS intensities of these main peaks (Figure S6b), showing that increased tryptophan was consistently associated with a lower kynurenine SERS signal.

We next aimed to employ SERS to monitor the impact of cell number (spheroid size) on the metabolic secretome. We thus traced the dynamics of tryptophan catabolism by SERS and compared our findings with a traditional metabolomic technique, such as ELISA. Initial SERS tests focused on associating the impact of spheroid size (studied by optical imaging) on their metabolic activity. Figures 2b,c and S7 show SERS spectra from both monoculture and STAM spheroids at all three predefined sizes (S, M, L), on day 14 after initial seeding. Analysis of the 760 cm^{-1} region revealed the presence of the peak associated with tryptophan, but identification of kynurenine-associated peaks was hindered by various interfering signals, likely originating from cell media molecules and ECM components interacting with the plasmonic substrate. This is in agreement with our previous experiments on 2D cell cultures, where Kyn could hardly be monitored in complex media, even in the absence of ECM-secreted components. We can thus conclude that the ECM produced during spheroid maturation hindered a reliable tracking of both elements of the catabolic pathway, thus requiring IDO-1 activity to be monitored using Trp consumption as an indirect indicator.

To assess the decrease in Trp concentration in STAM spheroids, a semiquantitative value was obtained by plotting the ratio between the intensities of the Trp peak (760 cm^{-1}) and a peak at 1029 cm^{-1} as a reference, which indicates interactions between the substrate and media components, like nicotinamide or niacinamide pyridine ring related vibrations and phenylalanine in-plane CH bending (Figure S8).[33,34] In Figure S9 we show a calibration curve resulting from the 760/1029 cm^{-1} intensity ratio, as a way of estimate the changes in Trp concentration and mitigate intersubstrate differences. The use of this internal control may help overcome the difficulties in maintaining absolute intensities for different disordered substrates, which may lead to different performance. Figure 2d reveals no discernible differences for Trp concentration in S-sized spheroids, for all three models. However, when increasing cell number, a tendency toward Trp consumption was

https://doi.org/10.1021/acssensors.4c01210
ACS Sens. 2024, 9, 4236−4247

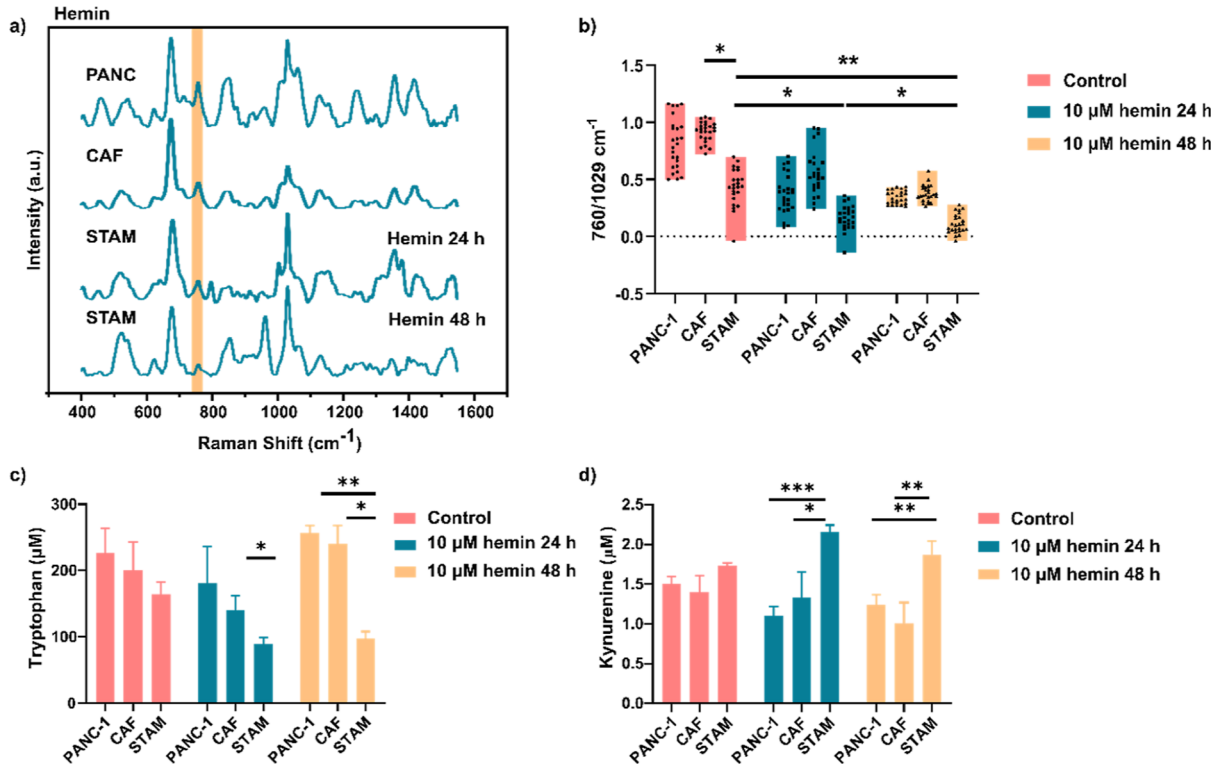

Figure 3. (a) SERS spectra for monoculture and STAM spheroids at M size, supplemented with 10 μM hemin for 24 and 48 h. (b) Analysis of the ratio between the peaks at 760 and 1029 cm^{-1}, based on 25 SERS spectra obtained from different hemin-treated spheroids. (c) ELISA results for tryptophan in hemin-treated spheroids. Hemin induced a significant decrease in extracellular tryptophan. (d) ELISA measurements revealing kynurenine levels in hemin-treated spheroids, showcasing high levels of the metabolite associated with hemin-derived tryptophan consumption. Data presented as mean ± SD *P < 0.05, **P < 0.01, ***P < 0.001.

observed in M-sized spheroids, culminating in a significant consumption of Trp for the larger size. Additionally, it should be noted that, in all experiments, we included monotypic spheroids as a negative control: (i) to prove that only Trp consumption can be observed in STAM spheroids, and (ii) to have a standard reference for Trp consumption. As a control, these results were complemented with ELISA analysis from the same supernatants, to confirm that the decrease in Trp was accompanied by an increase in extracellular Kyn. The trends observed in SERS spectra were mirrored in the Trp and Kyn ELISA assays, indicating a significant reduction of Trp metabolite concentration in M spheroids (Figure 2e). Concerning Kyn, a substantial production of the immunosuppressive metabolite in M-sized spheroids confirmed that the observed decrease in Trp resulted from the catabolic conversion. These results explain the absence of the Kyn peak in SERS spectra, potentially stemming from a combination of two effects: (i) the increased complexity of the medium in 3D cultures compared to 2D; and (ii) a lower induction of IDO-1 expression when compared to the artificial induction by IFN-γ supplementation, therefore accompanied by a lower concentration of extracellular Kyn. These findings, coupled with LD staining of the spheroids, prompted us to select the M size for subsequent measurements, to study the effect of different drugs on Trp consumption. These results underscored that SERS can be applied to spheroid monitoring and optimizing experimental conditions, with comparable results to ELISA experiments, but in a more rapid manner and avoiding sample destruction.

After optimizing spheroid size, we focused on the temporal evolution of spheroid metabolism. Previous experiments were conducted at 14 days postseeding. Therefore, we compared these results with data collected at earlier and later time-points during spheroid formation. We conducted measurements at two distinct time-points: an initial assessment at day 10 postseeding and a subsequent evaluation at day 21 postseeding. Figure S10 presents SERS spectra for both monoculture and STAM spheroids at these additional time-points. At day 10, only 3 days after the addition of the CAF cells to the STAM cancerous core, no significant reduction in tryptophan peak intensity was observed in STAM models, which is likely due to the need for a certain induction time to express IDO-1 and initiate metabolite conversion; both processes require several days to manifest themselves. At day 21, we could not discern any decrease in the average 760/1029 cm^{-1} ratio in STAM, compared to monoculture spheroids. We hypothesize that the loss of statistically significant consumption of Trp between 14 and 21 days could be correlated with the accumulation of stress from the increased formation of necrotic cores.[35] Our findings suggest that the optimal time point for studying fully developed spheroids with tryptophan-derived metabolic activity is still day 14, i.e., 1 week following the addition of CAFs to the STAM coculture spheroids.

SERS as a Drug Screening Tool. Next, we aimed to assess the impact of various drugs on tryptophan metabolic conversion, while exploring the suitability of SERS as a technique to assist drug selection. A notable challenge in drug testing arises from the use of dimethyl sulfoxide (DMSO), a

https://doi.org/10.1021/acssensors.4c01210
ACS Sens. 2024, 9, 4236−4247

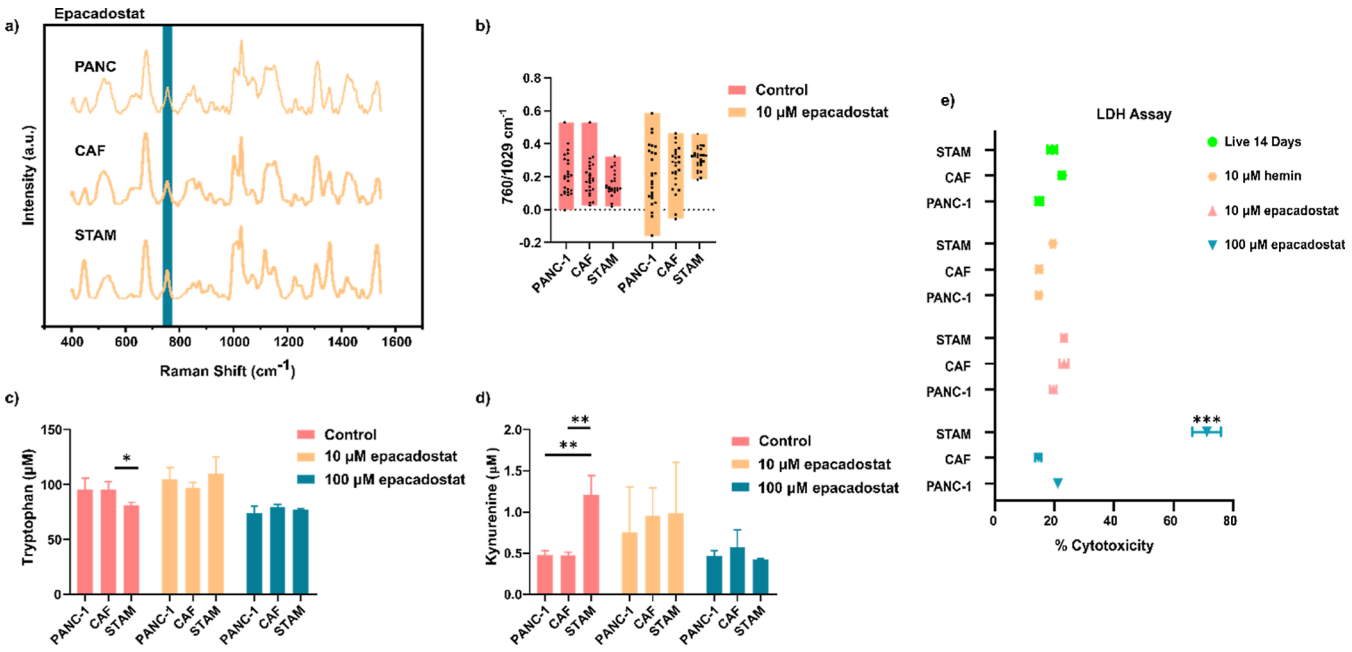

Figure 4. (a) SERS spectra for monoculture and STAM spheroids at M size, treated with 10 μM epacadostat for 48 h. (b) Analysis of the intensity ratio between the 760 and 1029 cm^{-1} peaks, based on 25 SERS spectra obtained from different epacadostat-treated spheroids. (c) ELISA results for tryptophan in epacadostat-treated spheroids. No tryptophan consumption could be detected after epacadostat treatment. (d) ELISA measurements revealing kynurenine levels in epacadostat-treated spheroids. These results resemble those of tryptophan, showing a decay in kynurenine release after drug treatment. (e) LDH cytotoxicity assay results for both monoculture and STAM spheroids, either in control conditions or treated with hemin and two epacadostat concentrations for 48 h in 14 days spheroids. Data presented as mean ± SD *P < 0.05, **P < 0.01, ***P < 0.001.

common solvent with a strong Raman signal, thereby posing challenges on the study of drugs dissolved in DMSO.[36]

We first selected hemin—an IDO-1 cofactor—to enhance enzyme activity and expedite the conversion of tryptophan into kynurenine. Simultaneously, to amplify the SERS signal, all spheroids were supplemented with 200 μM of tryptophan. Shown in Figure 3a are SERS spectra from monoculture spheroids treated with 10 μM of hemin for 24 h and STAM spheroids treated with the same drug concentration for both 24 and 48 h. A significant decrease in the 760 cm^{-1} peak was observed in STAM spheroids at 24 h of hemin treatment, which was further intensified at 48 h. Concurrently, the 680 cm^{-1} region revealed a distinctive peak associated with the presence of DMSO as a solvent of the hemin solution. SERS measurements of PANC-1 and CAF monoculture spheroids treated with hemin for 48 h are also presented in Figure S11. Consistent with the use of SERS to monitor spheroid size and temporal evolution, we plotted the 760/1029 cm^{-1} peak ratio, which revealed a significant decrease in tryptophan concentration in STAM spheroids under both control and hemin-treated conditions (Figure 3b). However, the values for this ratio were significantly lower when hemin was supplemented, especially when treated for 48 h. Complementary ELISA tests confirmed that, although there is a Trp decrease in nontreated STAM spheroids, significant consumption occurred only in spheroids treated with 10 μM hemin (Figure 3c). Finally, ELISA assays for kynurenine yielded results mirroring those of tryptophan, with a significant increase in the amount of this metabolite, observed only when hemin was employed to enhance IDO-1 activity (Figure 3d).

We subsequently directed our attention toward a drug with an effect opposite to that of hemin. We selected epacadostat, a clinically relevant, reversible competitive IDO-1 inhibitor, to investigate its impact on enzyme blockade.[14] The integration of epacadostat into our 3D models aimed to hinder enzyme activity, thereby disrupting the consumption of tryptophan and, consequently, the generation of kynurenine. We selected 10 μM as the treating condition, adhering to standard *in vitro* experimental protocols. The SERS spectra in Figure 4a reveal a prominent signal at 680 cm^{-1}, attributed to DMSO in the 10 μM epacadostat solution, as previously identified in hemin measurements (see Figure S12 for the SERS spectra of pure hemin and epacadostat under the screened conditions).

Analysis of the 760/1029 cm^{-1} ratios in Figure 4b revealed no significant differences between STAM and monoculture spheroids, when treated with the inhibitor—opposite to our previous observations with hemin. Additionally, ELISA assays for both tryptophan and kynurenine corroborate an impaired IDO-1 function, indicating similarities between monoculture and STAM epacadostat-treated spheroids, in line with the SERS results (Figure 4c,d). These experiments underscore a comparable efficacy between SERS and ELISA, both to monitor the tryptophan catabolic pathway in 3D and to evaluate drug testing.

Finally, we explored the effects of the tested drugs on cell viability at different concentrations, for all three models. Neither hemin nor epacadostat induced cell death at the screened concentration (10 μM) in any model. However, an intriguing effect was observed for higher doses of epacadostat (75 and 100 μM) on the STAM model—the only one expected to be affected by the drug due to the expression of IDO-1. In STAM spheroids, epacadostat selectively induced significant cell death in a dose-dependent manner (Figures 4e and S13). Approximately 40% cytotoxicity was observed in STAM spheroids treated with 75 μM epacadostat, and this effect increased to around 70% cytotoxicity at 100 μM. These unexpected effects warrant further investigation, as epacadostat is anticipated to interfere solely with the enzymatic activity of

https://doi.org/10.1021/acssensors.4c01210
ACS Sens. 2024, 9, 4236−4247

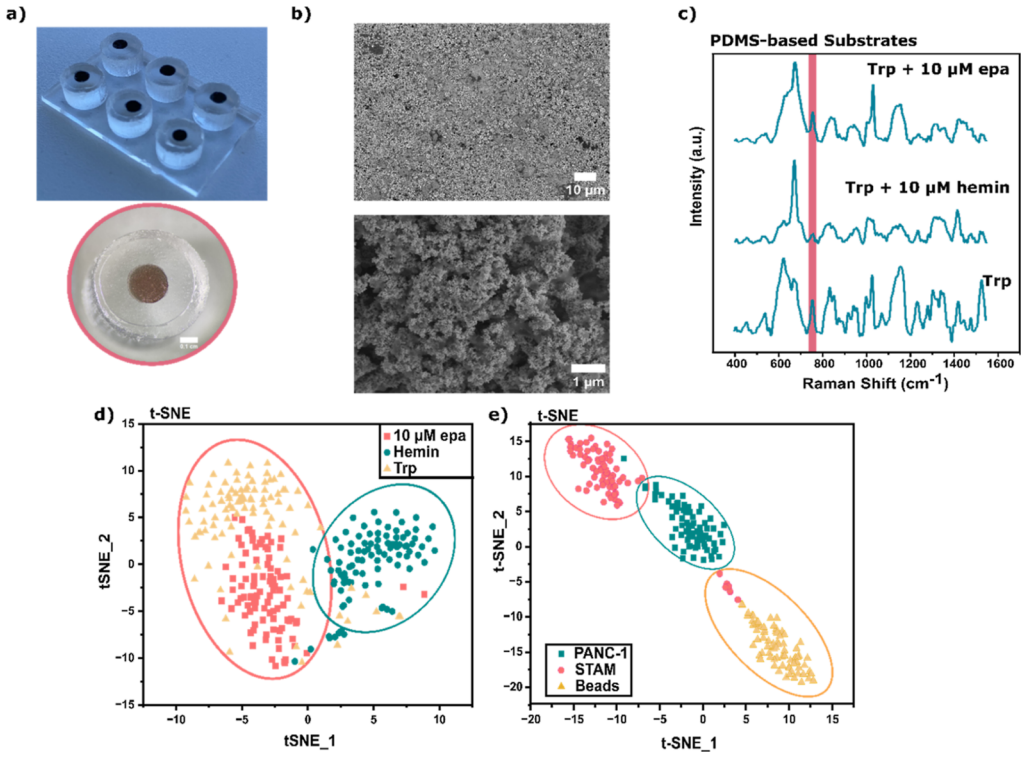

Figure 5. (a) Photograph of a 6 well PDMS array with drying drop SERS substrates and a zoomed image of the drying drop substrate on a PDMS lid support. (b) Representative SEM images of the drying drop substrate on PDMS lid support. (c) SERS spectra illustrating PANC-1 spheroids supplemented with tryptophan, and STAM spheroids supplemented with the metabolite + 10 μM hemin and 10 μM epacadostat on day 14, performed in PDMS-based substrates. (d) t-distributed stochastic neighbor embedding (t-SNE) analysis of 10 μM epacadostat, and 10 μM hemin STAM treated spheroids, and Trp-treated PANC-1 spheroids SERS spectra, obtained in PDMS-based drying drop substrates. (e) t-SNE analysis of PANC-1, STAM, and cancer-on-a-bead SERS spectra.

IDO-1 but not to induce cell death. The selective cytotoxicity observed for higher concentrations suggests potential avenues for targeted interventions in IDO-1-expressing cells or models.

Exploring the Synergy of High-Throughput Strategies, SERS and Unsupervised Machine Learning. Once the feasibility of applying SERS for tryptophan monitoring was proven, we directed our efforts toward expanding the application of SERS measurements in a noninvasive and high-throughput manner. Our initial protocol remained slow for high-throughput measurements because of the need to collect supernatants from cultured spheroids, to fabricate the substrates, and to incubate the collected supernatant with the plasmonic substrate for SERS measurements. Aiming to streamline this process and minimize intermediate steps, we devised a strategy involving custom-made lids for the well plates, incorporating SERS substrates. We thus customized a 96-well plate by 3D-printing stereolithography. The resulting resin plate served as a mold to obtain complementary polydimethylsiloxane (PDMS) lids, containing pillars that would penetrate each well and contact the spheroid culture supernatant. At the end of each pillar, SERS substrates were prepared by the drying drop strategy, to target molecules from the extracellular media (avoiding contact with the cell spheroids at the well bottom). This device allowed us to expose the plasmonic substrates to cellular supernatants, with no risk of spheroid disruption and cellular damage during media replacement, a challenge in fragile spheroid cultures. By simply removing the PDMS lid at the desired time, SERS spectra could be recorded to identify secreted metabolites with similar sensitivity to aluminum foil substrates. Shown in Figure 5a,b are 6-well PDMS lid models with plasmonic drying drop substrates on the pillars. PDMS lid supports of 15 wells are also shown in Figure S14. These substrates were tested on PANC-1 spheroids supplemented with Trp and STAM spheroids supplemented with Trp and treated with either 10 μM of hemin or 10 μM epacadostat (Figure 5c). SERS signals associated with tryptophan peaks were obtained from PDMS substrates in epacadostat-supplemented STAM spheroids, whereas they were consistently absent in hemin-treated STAM spheroids. The distribution maps from the pillar substrates (Figure S15) comprise 100 SERS spectra. The measurements obtained from these devices exhibited unique vibrational fingerprints for each drug screening condition (see Figure 5c), thereby allowing us to distinguish different clusters when applying the t-distributed stochastic neighbor embedding (t-SNE) technique (Figure 5d).[37] Such clusters correspond to the different conditions: (i) treatment with hemin, characterized by an increased Trp consumption; and (ii) 10 μM epacadostat with Trp supplementation, characterized by intense Trp-related signals. This spatial classification confirmed the importance of the applied treatments in the secreted profile of the spheroids, being able to discriminate between different conditions according to their ability to promote or block tryptophan consumption. Additionally, principal component analysis (PCA) of the obtained supernatants was performed (see Figure S16), indicating distinct clustering, particularly between hemin treated and tryptophan-supplemented spheroids and identifying significant differences throughout the whole spectra, not only based on Trp peaks.

https://doi.org/10.1021/acssensors.4c01210
ACS Sens. 2024, 9, 4236−4247

Finally, we assessed the use of SERS to discern more complex 3D models, on the basis of their secreted profiles. Following the same methodology as described above, we cultured pancreatic monoculture spheroids, STAM, and cancer-on-a-bead models. The cancer-on-a-bead model, as previously described,[24] involves a stratified coculture incorporating ECM components into different layers. The beads, formed on superhydrophobic surfaces, comprise a core layer of PANC-1 cells with gelatin methacrylate (GelMA) and a CAF shell with GelMA and hyaluronic acid methacrylate (HAMA). Supernatants from these models were collected at days 7 and 14 after seeding, and their metabolic profiles were analyzed using SERS. At day 7, no traces of tryptophan or kynurenine were detected. However, employing statistical PCA of the spectra, we could differentiate the cancer-on-a-bead models from those lacking an ECM component (Figure S17a,b). However, we could not detect any trace of the metabolic pathway. Upon analysis of the supernatants from spheroids cultured for 14 days, differences in the tryptophan peak did become evident. Pancreatic monotypic spheroids exhibited a considerably higher Trp SERS signal than that observed in both the cancer-on-a-bead system and STAM spheroids (Figure S17c). Subsequent PCA and t-SNE analyses allowed differentiation not only between the cancer-on-a-bead model and the spheroids, but also between mono- and coculture tumor−stroma spheroids, indicating different metabolic profiles (Figure 5e,d). This experiment underscores the efficacy of SERS in the classification and monitoring of cancer models, emphasizing the optimal culture time point to discern clear differences and conduct drug testing experiments.

CONCLUSIONS

We have demonstrated the potential of SERS as a versatile technique for deciphering metabolic communications within the dynamic landscape of the TME. SERS results were validated by ELISA, a traditional methodology, but with the additional advantages of being faster, simpler, and involving reduced pretreatment or separation steps. The application of SERS to monitor the tryptophan catabolic conversion into kynurenine not only served to optimize spheroid size, but also to identify the optimal time point for studying fully developed spheroids. Our results demonstrate the use of SERS in drug testing, providing a semiquantitative assessment of changes in tryptophan consumption induced by IDO-1, as well as by stimulating and inhibitory drugs. Building upon these results, integration of SERS within easily fabricated PDMS-based devices additionally allowed high-throughput and noninvasive measurements. This approach streamlined the experimental process, reducing potential cell disruption and spheroid damage during media exchange. Application of our system could lead to highly streamlined approaches for SERS monitoring in various disease models. Moreover, incorporation of unsupervised data analysis enabled effective clustering of samples, enhancing the interpretability of complex metabolic interactions within the TME. Overall, we conclude that SERS has become a versatile tool for probing intricate cellular processes and unraveling drug response within the context of complex pancreatic 3D tumor−stroma models.

ASSOCIATED CONTENT

Supporting Information

The Supporting Information is available free of charge at https://pubs.acs.org/doi/10.1021/acssensors.4c01210.

Additional optical spheroids pictures, nanoparticles characterization, additional LDH, SERS measurements and PCA analyses (PDF)

AUTHOR INFORMATION

Corresponding Author

Luis M. Liz-Marzán − *CIC biomaGUNE, Basque Research and Technology Alliance (BRTA), 20014 Donostia-San Sebastián, Spain; Centro de Investigación Biomédica en Red de Bioingeniería, Biomateriales y Nanomedicina (CIBER-BBN), 20014 Donostia-San Sebastián, Spain; Ikerbasque, Basque Foundation for Science, 48009 Bilbao, Spain; Cinbio, Universidade de Vigo, 36310 Vigo, Spain;* orcid.org/0000-0002-6647-1353; Email: llizmarzan@cicbiomagune.es

Authors

Pablo S. Valera − *CIC biomaGUNE, Basque Research and Technology Alliance (BRTA), 20014 Donostia-San Sebastián, Spain; Centro de Investigación Biomédica en Red de Bioingeniería, Biomateriales y Nanomedicina (CIBER-BBN), 20014 Donostia-San Sebastián, Spain; CIC bioGUNE, Basque Research and Technology Alliance (BRTA), 48160 Derio, Spain; Departamento de Química Aplicada, Universidad del País Vasco/Euskal Herriko Universitatea (UPV/EHU), 20018 Donostia-San Sebastián, Spain*

Margarida Henriques-Pereira − *Department of Chemistry, CICECO-Aveiro Institute of Materials, University of Aveiro Campus Universitário de Santiago, 3810-193 Aveiro, Portugal*

Marita Wagner − *CIC biomaGUNE, Basque Research and Technology Alliance (BRTA), 20014 Donostia-San Sebastián, Spain; Departamento de Química Aplicada, Universidad del País Vasco/Euskal Herriko Universitatea (UPV/EHU), 20018 Donostia-San Sebastián, Spain; CIC nanoGUNE, Basque Research and Technology Alliance (BRTA), 20018 Donostia-San Sebastián, Spain*

Vítor M. Gaspar − *Department of Chemistry, CICECO-Aveiro Institute of Materials, University of Aveiro Campus Universitário de Santiago, 3810-193 Aveiro, Portugal;* orcid.org/0000-0002-0372-2493

João F. Mano − *Department of Chemistry, CICECO-Aveiro Institute of Materials, University of Aveiro Campus Universitário de Santiago, 3810-193 Aveiro, Portugal;* orcid.org/0000-0002-2342-3765

Complete contact information is available at: https://pubs.acs.org/10.1021/acssensors.4c01210

Author Contributions

○P.S.V. and M.H.-P. contributed equally. P.S.V., M.H.P., V.M.G., J.F.M., and L.M.L.-M. designed research; P.S.V., M.H.P., and M.W. performed research; P.S.V., and M.H.P. analyzed data; and P.S.V., M.H.P., V.M.G., J.F.M., and L.M.L.-M. wrote the paper.

Funding

L.M.L.-M. acknowledges funding from the European Research Council (ERC AdG 787510, 4DbioSERS). This work was developed within the scope of the project CICECO-Aveiro Institute of Materials, UIDB/50011/2020 (doi: 10.54499/UIDB/50011/2020), UIDP/50011/2020 (doi: 10.54499/UIDP/50011/2020) & LA/P/0006/2020 (doi: 10.54499/

LA/P/0006/2020), financed by national funds through the FCT/MCTES (PIDDAC).

Notes

The authors declare no competing financial interest.

■ ABBREVIATIONS

TME	tumor microenvironment
ECM	extracellular matrix
PDAC	pancreatic ductal adenocarcinoma
CAF	cancer-associated fibroblasts
Trp	tryptophan
Kyn	kynurenine
IDO-1	indoleamine 2,3 dioxygenase
TDO	tryptophan 2,3 dioxygenase
NAD	nicotinamide adenine dinucleotide
AhR	aryl hydrocarbon receptor
DC	dendritic cells
LC−MS	liquid chromatography−coupled mass spectrometry
NMR	nuclear magnetic resonance
SERS	surface-enhanced Raman spectroscopy
2D	two-dimensional
3D	three-dimensional
SEM	scanning electron microscopy
TEM	transmission electron microscopy
NP	nanoparticle
HBSS	Hanks' balanced salt solution
DMEM	Dulbecco's modified eagle medium
IFN-γ	interferon-gamma
STAM	stratified pancreatic cancer−stroma spheroids
LD	live and dead
IL-6	interleukin 6
IL-8	interleukin 8
CXCL1	chemokine (C-X-C motif) ligand 1
ELISA	enzyme-linked immunosorbent assay
DMSO	dimethyl sulfoxide
LDH	lactate dehydrogenase
PDMS	polydimethylsiloxane
t-SNE	t-distributed stochastic neighbor embedding
GelMA	gelatin methacrylate
HAMA	hyaluronic acid methacrylate
PCA	principal component analysis
ULA	ultralow adhesion
GAPDH	glyceraldehyde-3-phosphate dehydrogenase
SLA	stereolithography
UV	ultraviolet
SEM	scanning electron microscopy

■ REFERENCES

(1) Hanahan, D.; Weinberg, R. A. Hallmarks of cancer: the next generation. *Cell* **2011**, *144*, 646−674.
(2) Lyssiotis, C. A.; Kimmelman, A. C. Metabolic Interactions in the Tumor Microenvironment. *Trends Cell Biol.* **2017**, *27*, 863−875.
(3) Tiwari, A.; Trivedi, R.; Lin, S.-Y. Tumor Microenvironment: Barrier or Opportunity towards Effective Cancer Therapy. *J. Biomed. Sci.* **2022**, *29*, 83.
(4) Mayer, S.; Milo, T.; Isaacson, A.; Halperin, C.; Miyara, S.; Stein, Y.; Lior, C.; Pevsner-Fischer, M.; Tzahor, E.; Mayo, A.; Alon, U.; Scherz-Shouval, R. The Tumor Microenvironment Shows a Hierarchy of Cell-Cell Interactions Dominated by Fibroblasts. *Nat. Commun.* **2023**, *14*, 5810.
(5) Halbrook, C. J.; Lyssiotis, C. A.; Pasca di Magliano, M.; Maitra, A. Pancreatic Cancer: Advances and Challenges. *Cell* **2023**, *186*, 1729−1754.
(6) Zhang, T.; Ren, Y.; Yang, P.; Wang, J.; Zhou, H. Cancer-Associated Fibroblasts in Pancreatic Ductal Adenocarcinoma. *Cell Death Dis.* **2022**, *13*, 897.
(7) Tian, C.; Huang, Y.; Clauser, K. R.; Rickelt, S.; Lau, A. N.; Carr, S. A.; Vander Heiden, M. G.; Hynes, R. O. Suppression of pancreatic ductal adenocarcinoma growth and metastasis by fibrillar collagens produced selectively by tumor cells. *Nat. Commun.* **2021**, *12*, 2328.
(8) Shi, R.; Tang, Y.; Miao, H. Metabolism in Tumor Microenvironment: Implications for Cancer Immunotherapy. *MedComm* **2020**, *1*, 47−68.
(9) Francescone, R.; Crawford, H. C.; Vendramini-Costa, D. B. Rethinking the Roles of Cancer-Associated Fibroblasts in Pancreatic Cancer. *Cell. Mol. Gastroenterol. Hepatol.* **2024**, *17* (5), 737−743.
(10) Rebelo, R.; Xavier, C. P. R.; Giovanetti, E.; Vasconcelos, M. H. Fibroblasts in Pancreatic Cancer: Molecular and Clinical Perspectives. *Trends Mol. Med.* **2023**, *29*, 439−453.
(11) Xue, C.; Li, G.; Zheng, Q.; Gu, X.; Shi, Q.; Su, Y.; Chu, Q.; Yuan, X.; Bao, Z.; Lu, J.; Li, L. Tryptophan Metabolism in Health and Disease. *Cell Metab.* **2023**, *35*, 1304−1326.
(12) Kim, M.; Tomek, P. Tryptophan: A Rheostat of Cancer Immune Escape Mediated by Immunosuppressive Enzymes IDO1 and TDO. *Front. Immunol.* **2021**, *12*, 636081.
(13) Dean, J. W.; Helm, E. Y.; Fu, Z.; Xiong, L.; Sun, N.; Oliff, K. N.; Muehlbauer, M.; Avram, D.; Zhou, L. The Aryl Hydrocarbon Receptor Cell Intrinsically Promotes Resident Memory CD8+ T Cell Differentiation and Function. *Cell Rep.* **2023**, *42*, 111963.
(14) Panfili, E.; Mondanelli, G.; Orabona, C.; Gargaro, M.; Volpi, C.; Belladonna, M. L.; Rossini, S.; Suvieri, C.; Pallotta, M. T. The catalytic inhibitor epacadostat can affect the non-enzymatic function of IDO1. *Front. Immunol.* **2023**, *14*, 1134551.
(15) Suri, G. S.; Kaur, G.; Carbone, G. M.; Shinde, D. Metabolomics in Oncology. *Cancer Rep.* **2023**, *6*, No. e1795.
(16) Danzi, F.; Pacchiana, R.; Mafficini, A.; Scupoli, M. T.; Scarpa, A.; Donadelli, M.; Fiore, A. To Metabolomics and Beyond: A Technological Portfolio to Investigate Cancer Metabolism. *Signal Transduction Targeted Ther.* **2023**, *8*, 137.
(17) Plou, J.; García, I.; Charconnet, M.; Astobiza, I.; García-Astrain, C.; Matricardi, C.; Mihi, A.; Carracedo, A.; Liz-Marzán, L. M. Multiplex SERS Detection of Metabolic Alterations in Tumor Extracellular Media. *Adv. Funct. Mater.* **2020**, *30*, 201910335.
(18) Valera, P. S.; Plou, J.; García, I.; Astobiza, I.; Viera, C.; Aransay, A.; Martin, J. E.; Sasselli, I. R.; Carracedo, A.; Liz-Marzán, L. M. SERS Analysis of Cancer Cell-Secreted Purines Reveals a Unique Paracrine Crosstalk in MTAP-Deficient Tumors. *Proc. Natl. Acad. Sci. U.S.A.* **2023**, *120*, No. e2311674120.
(19) Langer, J.; Jimenez de Aberasturi, D.; Aizpurua, J.; Alvarez-Puebla, R. A.; Auguié, B.; Baumberg, J. J.; Bazan, G. C.; Bell, S. E. J.; Boisen, A.; Brolo, A. G.; Choo, J.; Cialla-May, D.; Deckert, V.; Fabris, L.; Faulds, K.; García de Abajo, F. J.; Goodacre, R.; Graham, D.; Haes, A. J.; Haynes, C. L.; Huck, C.; Itoh, T.; Käll, M.; Kneipp, J.; Kotov, N. A.; Kuang, H.; Le Ru, E. C.; Lee, H. K.; Li, J.-F.; Ling, X. Y.; Maier, S. A.; Mayerhöfer, T.; Moskovits, M.; Murakoshi, K.; Nam, J.-M.; Nie, S.; Ozaki, Y.; Pastoriza-Santos, I.; Perez-Juste, J.; Popp, J.; Pucci, A.; Reich, S.; Ren, B.; Schatz, G. C.; Shegai, T.; Schlücker, S.; Tay, L.-L.; Thomas, K. G.; Tian, Z.-Q.; Van Duyne, R. P.; Vo-Dinh, T.; Wang, Y.; Willets, K. A.; Xu, C.; Xu, H.; Xu, Y.; Yamamoto, Y. S.; Zhao, B.; Liz-Marzán, L. M. Present and Future of Surface-Enhanced Raman Scattering. *ACS Nano* **2020**, *14*, 28−117.
(20) Ferreira, L. P.; Gaspar, V. M.; Mano, J. F. Design of Spherically Structured 3D In Vitro Tumor Models -Advances and Prospects. *Acta Biomater.* **2018**, *75*, 11−34.
(21) Lagies, S.; Schlimpert, M.; Neumann, S.; Wäldin, A.; Kammerer, B.; Borner, C.; Peintner, L. Cells Grown in Three-Dimensional Spheroids Mirror In Vivo Metabolic Response of Epithelial Cells. *Commun. Biol.* **2020**, *3*, 246.
(22) Kapałczyńska, M.; Kolenda, T.; Przybyła, W.; Zajączkowska, M.; Teresiak, A.; Filas, V.; Ibbs, M.; Bliźniak, R.; Łuczewski, Ł.; Lamperska, K. 2D and 3D Cell Cultures − a Comparison of Different Types of Cancer Cell Cultures. *Arch. Med. Sci.* **2016**, *14*, 910−919.

https://doi.org/10.1021/acssensors.4c01210
ACS Sens. 2024, 9, 4236−4247

(23) Monteiro, M. V.; Ferreira, L. P.; Rocha, M.; Gaspar, V. M.; Mano, J. F. Advances in Bioengineering Pancreatic Tumor-Stroma Physiomimetic Biomodels. *Biomaterials* **2022**, *287*, 121653.
(24) Monteiro, M. V.; Rocha, M.; Gaspar, V. M.; Mano, J. F. Programmable Living Units for Emulating Pancreatic Tumor-Stroma Interplay. *Adv. Healthcare Mater.* **2022**, *11*, 202102574.
(25) Bastús, N. G.; Comenge, J.; Puntes, V. Kinetically Controlled Seeded Growth Synthesis of Citrate-Stabilized Gold Nanoparticles of up to 200 nm: Size Focusing versus Ostwald Ripening. *Langmuir* **2011**, *27*, 11098−11105.
(26) Hagemann, C.; Bailey, M. C. D.; Carraro, E.; Lionello, V. M.; Khokar, N.; Tedesco, F. S.; Serio, A. SOL3D: Soft-Lithography on 3D Vat Polymerised Moulds for Fast, Versatile, and Accessible High-Resolution Fabrication of Customised Multiscale Cell Culture Devices with Complex Designs, **2023**. bioRxiv 2022.02.22.481424.
(27) Ivanov, D. P.; Parker, T. L.; Walker, D. A.; Alexander, C.; Ashford, M. B.; Gellert, P. R.; Garnett, M. C. Multiplexing Spheroid Volume, Resazurin and Acid Phosphatase Viability Assays for High-Throughput Screening of Tumour Spheroids and Stem Cell Neurospheres. *PLoS One* **2014**, *9*, No. e103817.
(28) Sherman, M. H.; di Magliano, M. P. Cancer-Associated Fibroblasts: Lessons from Pancreatic Cancer. *Annu. Rev. Cancer Biol.* **2023**, *7*, 43−55.
(29) Tanaka, T.; Narazaki, M.; Kishimoto, T. IL-6 in Inflammation, Immunity, and Disease. *Cold Spring Harb. Perspect. Biol.* **2014**, *6*, a016295.
(30) Sawant, K. V.; Poluri, K. M.; Dutta, A. K.; Sepuru, K. M.; Troshkina, A.; Garofalo, R. P.; Rajarathnam, K. Chemokine CXCL1Mediated Neutrophil Recruitment: Role of Glycosaminoglycan Interactions. *Sci. Rep.* **2016**, *6*, 33123.
(31) Pease, J. E.; Sabroe, I. The Role of Interleukin-8 and its Receptors in Inflammatory Lung Disease: Implications for Therapy. *Am. J. Respir. Med.* **2002**, *1*, 19−25.
(32) Sherman, L. M.; Petrov, A. P.; Karger, L. F. P.; Tetrick, M. G.; Dovichi, N. J.; Camden, J. P. A Surface-Enhanced Raman Spectroscopy Database of 63 Metabolites. *Talanta* **2020**, *210*, 120645.
(33) Jaworska, A.; Fornasaro, S.; Sergo, V.; Bonifacio, A. Potential of Surface Enhanced Raman Spectroscopy (SERS) in Therapeutic Drug Monitoring (TDM). A Critical Review. *Biosensors* **2016**, *6*, 47.
(34) Jeffers, R. B.; Cooper, J. B. FT-Surface-Enhanced Raman Scattering of Phenylalanine Using Silver-Coated Glass Fiber Filters. *Spectrosc. Lett.* **2010**, *43*, 220−225.
(35) Browning, A. P.; Sharp, J. A.; Murphy, R. J.; Gunasingh, G.; Lawson, B.; Burrage, K.; Haass, N. K.; Simpson, M. Quantitative Analysis of Tumour Spheroid Structure. *eLife* **2021**, *10*, No. e73020.
(36) Han, X.-B.; Ye, S. Structural Design of Oxygen Reduction Redox Mediators (ORRMs) Based on Anthraquinone (AQ) for the Li−O_2 Battery. *ACS Catal.* **2020**, *10*, 9790−9803.
(37) Van der Maaten, L.; Hinton, G. Viualizing Data Using t-SNE. *J. Mach. Learn. Res.* **2008**, *9*, 2579−2605.

https://doi.org/10.1021/acssensors.4c01210
ACS Sens. 2024, 9, 4236−4247